Applied Nano Materials, Available online 5 April 2024
DOI: 10.1021/acsanm.4c00674

Label-Free Analysis of Protein Biomarkers Using Pattern-optimized Graphene-Nanopyramid SERS for Rapid Diagnosis of Alzheimer's Disease

*Heping Wu[1], Yan Duan[2,3], Luyue Jiang[1], Xinhao Cao[1], Zhen Xie[2,] *, Yi Quan[4], Matthew Xinhu Ren[5], Shengli Wu[6], Nan Zhang[1], Zhugen Yang[7], Libo Zhao[8,] *, Zhuangde Jiang[9], Gang Zhao[2,] * Wei Ren[1,9] *, Gang Niu[1,9] **

[1] State Key Laboratory for Manufacturing Systems Engineering; Electronic Materials Research Laboratory, Key Laboratory of the Ministry of Education, School of Electronic Science and Engineering, Xi'an Jiaotong University, 710049 Xi'an, China

[2] The College of Life Sciences and Medicine, Northwest University, No. 229 Taibai North Road, Xi'an, Shaanxi, 710069, P.R. China

[3] Department of Clinical Laboratory, Xi'an Daxing Hospital, Xi'an 710016, China.

[4] School of Microelectronics, Xidian University, Xi'An, 710071, China

[5] Biology Program, Faculty of Science, The University of British Columbia, Vancouver, BC V6T 1Z4, Canada

[6] Key Laboratory of Physical Electronics and Devices, Ministry of Education, School of Electronic Science and Engineering, Xi'an Jiaotong University, Xi'an, 710049, China

[7] Cranfield Water Science Institute, School of Water, Energy and Environment, Cranfield University, Cranfield, MK43 0AL, UK

[8] School of Instrument Science and Technology, State Key Laboratory for Manufacturing Systems Engineering & The International Joint Laboratory for Micro/Nano Manufacturing and Measurement Technology, Xi'an Jiaotong University,Xi'an, 710049, China

[9] The State Key Laboratory for Manufacturing Systems Engineering & The International Joint Laboratory for Micro/Nano Manufacturing and Measurement Technology, Xi'an Jiaotong University, Xi'an 710049, China

*Gang Niu. E-mail: gangniu@xjtu.edu.cn.

*Wei Ren. E-mail: wren@mail.xjtu.edu.cn.

*Gang Zhao. E-mail: zhaogang@nwu.edu.cn.

*Libo Zhao. E-mail: libozhao@mail.xjtu.edu.cn.

*Zhen Xie. E-mail: xiezhenhh@163.com.

ABSTRACT

The quantitative and highly sensitive detection of biomarkers such as Tau proteins and Aβ polypeptides is considered one of the most effective methods for the early diagnosis of Alzheimer's Disease (AD). Surface-enhanced Raman spectroscopy (SERS) detection is a promising method, which faces, however, challenges like insufficient sensitivity due to the non-optimized nanostructures for specialized analytes sizes and insufficient control of the location of SERS hot spots. Thus the SERS detection of AD biomarkers is restricted. We reported here an in-depth study of the analytical Raman enhancement factor (EF) of the wafer-scale graphene-Au nanopyramid hybrid SERS substrates, using the combination of both theoretical calculation and experimental measurements. Experimental results show that larger nanopyramids and smaller gap spacing lead to larger SERS EF, with an optimized analytical EF up to 1.1×10^{10}. The hybrid SERS substrate exhibited detection limits of 10^{-15} M for Tau and phospho-Tau (P-Tau) proteins and 10^{-14} M for Aβ polypeptides, respectively. Principal component analysis correctly categorized the SERS spectra of different biomarkers at ultra-low concentrations (10^{-13} M) using the optimized substrate. Amide III bands at 1200 cm^{-1} to 1300 cm^{-1} reflect different structural conformations of proteins or polypeptides. Tau and P-Tau proteins are inherently disordered with a few α-helix residuals. The structure of Aβ42 polypeptides transitioned from α-helix to β-sheet as the concentration increased. These results demonstrate that the hybrid SERS method could be a simple

and effective way for the label-free detection of protein biomarkers to enable rapid early diagnosis of AD and other diseases.

Keywords: label-free detection, surface-enhanced Raman spectroscopy, Alzheimer's disease, phospho-Tau protein, Aβ42 polypeptide, protein secondary structure

1. Introduction

Alzheimer's disease (AD) is a common neurodegenerative disease characterized by memory loss and cognitive impairment. AD affects more than 50 million people worldwide currently, with about 135 million people expected to develop by 2050.[1-2] Despite impressive efforts over the past 30 years, there are still no treatments to modify and cure the disease.[3] Brain imaging and neuropsychological testing are two significant clinical diagnostic methods for AD. Brain imaging examinations show characteristic changes in the brains of patients.[4] Neuropsychological testing could establish cognitive impairment.[5] The current research on AD is mainly concentrated on interventions to prevent the onset and progression,[3] which makes the early diagnosis quite significant. The core pathological biomarkers for AD include total tau protein, indicating the extent of neurodegeneration; phospho-Tau (P-Tau) protein, associated with neurofibrillary pathological changes; and amyloid β42 (Aβ42) peptide, indicative of cortical amyloid deposition.[6] These core biomarkers have high diagnostic accuracy, with sensitivity and specificity of 85-90%, to identify prodromal AD in the mild cognitive impairment stage.[7] Quantitative and highly sensitive detection of proteins is widely studied. To date, the detection of AD biomarkers is mostly based on the measurement of specific light absorption, such as enzyme-linked immunosorbent assay (ELISA) method, local surface plasmon resonance technology, or chromatography.[8] However, these

methods suffer from issues such as time-consuming, limited resolution or sensitivity, and expensive equipment.[9]

Surface-enhanced Raman spectroscopy (SERS) is a powerful vibrational spectroscopy technique that enables highly sensitive detection of analytes at low concentrations.[10-11] The generally accepted mechanisms of SERS include electromagnetic enhancement and chemical enhancement.[12] The application of SERS in protein detection has been widely studied. Zhu et al. developed a SERS aptasensor based on a hydrophobic assembled nanoacorn with improved reproducibility and reduced nonspecific binding effect,[13] and then demonstrated the ability of the substrate to profile well-characterized exosome proteins including CD63, HER2 and EpCAM. Ma et al. modified Ag nanoparticles with different metal ions as SERS substrates, and investigated the SERS spectra of Tau proteins phosphorylated at different sites.[14] Park et al. detected the AD markers Tau protein and Aβ42 peptide using three-dimensional (3D) gold nanowire arrays prepared by nanoimprinting as solid SERS substrates, and obtained the limit of detections (LODs) of 10^{-11} moles per liter (M) and 10^{-9} M of the two biomarkers, respectively, corresponding to a SERS enhancement factor (EF) of 5.5×10^{5}.[15] Xie group investigated the self-association and LODs of Aβ peptides in detail,[16-17] and further demonstrated a convolutional neural network-based AD diagnosis approach using the SERS fingerprints of human cerebrospinal fluid (CSF).[18] Compared with conventional disease diagnosis methods such as ELISA, chromatography, and mass spectrometry, SERS technology has the advantages of high sensitivity and convenience of detection and analysis, which makes it highly promising in the early diagnosis of some intractable diseases such as AD.[15]

High-performance substrate paves the way for the application of SERS technology.[19] Nano-pyramidal SERS substrate is a universal platform with label-free detection capability, and related

research has been carried out. Jiang et al. first fabricated large-scale metallic nanopyramid arrays based on non-close-packed SiO_2 two-dimensional (2D) colloidal crystals.[20-21] However, the preparation of 2D colloidal crystals by spin coating required precise control of the parameters as well as the concentration of colloidal dispersion, and thus was very difficult to operate.[22] Xie et al. improved the preparation process and fabricated large-area nanopyramid arrays based on two-dimensional colloidal crystals of polystyrene (PS) microspheres prepared by self-assembly on the water surface.[23] Graphene monolayer was then transferred on the nanopyramid substrate to construct a graphene-Au nanopyramid (GAuNP) hybrid SERS platform, which excelled in the detection of various biochemical molecules. Our group has further improved the large-area uniformity of the hybrid SERS substrate by introducing the Langmuir-Blodgett method,[24] and performed high-cleanliness graphene transfer by using PMMA/paraffin as the supporting layer.[25] We have also proved the nanopyramidal SERS substrates exhibit excellent structural uniformity, spectral uniformity, stability as well as reliability.[24] However, the impact of nanopyramid size and gap distance on the SERS-enhanced performance of the hybrid system is still lacking. The size of the nanostructures has a decisive effect on the SERS EF.[26] Weaker Raman signals by non-optimized SERS biochips could be challenges for the quantitative detection, identification and structure analysis of protein molecules. Thus it is necessary to optimize the size of the nanopyramids and the sensitivity of the hybrid platform.

In this study, we investigated the impact of nanopyramid size and gap spacing on the electromagnetic field enhancement of the GAuNP hybrid SERS substrates by FDTD simulations. Using colloidal lithography and a series of micro-nano fabrication processes, four types of GAuNP SERS substrates with different pyramid sizes and pitches were fabricated. Based on the pattern-optimized SERS substrate and principal component analysis (PCA) method, we have achieved

breakthroughs in label-free structure analysis, quantification, and species identification of three types of important AD biomarkers, which demonstrates the versatility of the SERS substrates. Compared with traditional methods such as ELISA, this protocol does not require elaborate sample preparation and complex analysis procedures, nuclear magnetic resonance, and cryo-electron microscopy, and is of significance for the early ultrasensitive diagnosis of AD.

2. Experimental Section

2.1. FDTD simulation. 3D FDTD simulation was performed to calculate the electromagnetic field distribution of the Au nanopyramidal substrates. Models composed of two Au nanopyramids were built and the conformal mesh size was set down to 0.5 nm (x, y, and z directions). The curved graphene model prebuilt in the 3D modeling software was imported to FDTD solutions in the STL format. The optical constants of materials were taken from Ref.[27-28] The perfectly matched layer boundary condition was applied in all directions. The amplitude $|E_0|$ of the incident light is 1.

2.2. Au nanopyramidal substrate fabrication. The SERS substrates composed of Au nanopyramids were fabricated by colloidal lithography and a series of modern semiconductor nanofabrication processes. PS microspheres, Cr layer and the SiO_2 layer were successively used as masks to perform the dry and wet etching. Other techniques used include E-Beam deposition, lift-off, magnetron sputtering, and graphene transfer.[24] Fig. S1 shows the schematic illustration of the process. The commercial chemical vapor deposition (CVD) graphene was purchased from Wuxi Huicheng Graphene Tech&Appl Co., Ltd. Nanopyramids with different bottom side lengths and spacings were realized by precisely controlling the

diameter of the PS microspheres. Other details of the process can be found in our prior publications.[22, 24]

2.3. Preparation of the SERS samples. R6G and Aβ42 peptides were purchased from Sigma (Shanghai, China), Tau and P-Tau proteins were purchased from novoprotein (Suzhou, China) and Abcam (Shanghai, China), respectively. The molecules were dissolved in de-ionic (DI) water. R6G solution at 10^{-2} M was firstly prepared, and then diluted 10-fold in sequence to prepare solutions at other concentrations. Protein solutions at 10^{-6} M were firstly prepared and then diluted 10-fold in sequence. 10 μL aqueous solution of each chemical was dropped onto the graphene hybrid SERS substrate in 5 times and detected after drying.

2.4. Characterization methods. Scanning electron microscope (SEM) measurements were performed by an FEI Quanta FEG 250, with an acceleration voltage of 10 kV. Raman spectra were acquired with a LabRAM HR Evolution (Horiba) Raman microscope system, equipped with a standard 633 nm laser. The single spectral power was kept at 1.75 mW with 600 lines/mm grating. Raman spectra in this study have been baseline corrected and averaged.

3. Results and Discussion

3.1. FDTD simulation of the nanopyramidal substrate.

The Au nanopyramidal SERS substrates have been studied by several groups,[21, 23] however, the size effect study is still lacking. This is significant for the SERS because the size of the nanostructures strongly affects the EF of the SERS substrate.[29] To clarify the impact of the nanopyramid size and gap distance, we simulated the electromagnetic field enhancement of Au nanopyramid substrates with different sizes by FDTD simulation. The FDTD method is based on

Maxwell's equations (Eq. 1 and 2), solving the numerical solution by differential discretization.[30] In Cartesian coordinates, Maxwell's curl equation can be expressed into scalar equations as Eq. SE1 and SE2. The electric and magnetic fields alternate with time. Maxwell's equations were further discretized into difference form by taking a half-time step (Eq. SE3). Each field component of $\vec{E}$ and $\vec{H}$ can be solved alternately on a discrete spatial and temporal grid cell, and the electromagnetic field in space at a later time can be obtained.[31]

$$\nabla \times \vec{E} = -\frac{\partial \vec{B}}{\partial t} \tag{1}$$

$$\nabla \times \vec{H} = \vec{J} + \frac{\partial \vec{D}}{\partial t} \tag{2}$$

where $\vec{E}$, $\vec{D}$, $\vec{H}$, $\vec{B}$, and $\vec{J}$ are the electric field intensity vector, electric displacement vector, magnetic field intensity vector, magnetic induction intensity vector and current density vector, respectively. In an isotropic medium, the relationships between the above physical quantities are shown in Eq. 3.

$$\vec{D} = \varepsilon \vec{E}, \quad \vec{B} = \mu \vec{H}, \quad \vec{J} = \sigma \vec{E} \tag{3}$$

where ε, μ, σ are the medium dielectric constant, magnetic permeability coefficient and electrical conductivity, respectively.

Fig. 1a illustrates the model consisting of two Au nanopyramids with a conformal curved graphene monolayer on its surface. Figure 1b is a contour plot of the maximum value of the electromagnetic field strengths for Au pyramid arrays with different pyramid gaps (X-axis) and pyramid bottom side lengths (Y-axis). The theoretical EF of the SERS substrate is proportional to $|E|^4$.[32] It can be seen in Fig. 1b that the highest electromagnetic field strengths gradually augmented

from the lower left to the upper right (the color changes from blue to red), which suggests that larger nanopyramid sizes and smaller gap distances facilitate the increase of SERS EF. The nanopyramid substrates with sizes in the dark gray region in Fig. 1b are not available using colloidal lithography method due to the limitation of the PS ball size (Fig. S2). The dashed black line with a slope of 2.41 shows the critical line, on which the larger the nanopyramid is, the higher the EF value is. The theoretical EFs of the four nanopyramids SERS substrates marked in Fig. 1b (#1 to #4) are 9.0×10^8, 1.8×10^8, 5.5×10^7, and 1.5×10^6, respectively. Moreover, we found that the theoretical EFs of GAuNP substrate and AuNP substrate are rather similar.[24] This suggests the contribution of graphene to the SERS enhancement mainly lies in the chemical enhancement mechanism, which cannot be revealed by FDTD simulation.[33]

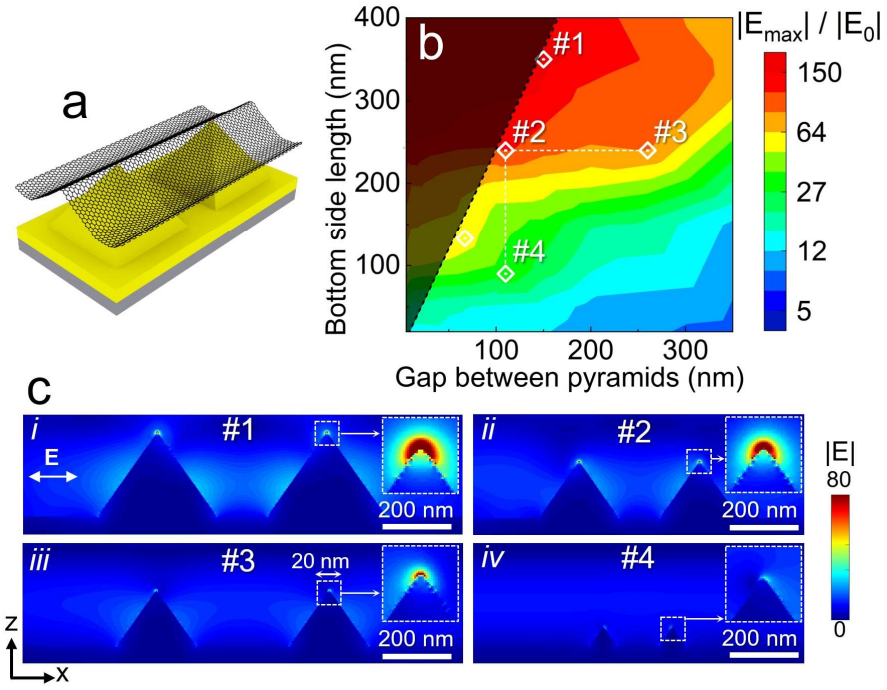

Figure 1. The electromagnetic field distributions of the GAuNP substrates by FDTD simulation. a. The model of the GAuNP substrate. b. Contour plots of the highest electromagnetic field strengths for GAuNP substrates with different pyramid sizes and gap distances. c. Electromagnetic field

distributions on the x-z cross-sections of the four samples in Fig. 1b. Insets (the side length is 20 nm) show the enlarged views of the apex regions of the nanopyramids.

The distribution of electromagnetic fields of single nanopyramids with different sizes was also studied. Fig. 1c (i-iv) shows the distributions of the enhanced electromagnetic fields on the x-z cross-section of #1 ~ #4 nanopyramidal substrates, respectively. The maximum electromagnetic field enhancement of the nanopyramid-type SERS substrate mainly gathered on the pyramid apex region, which is the "hot spot" of the SERS substrate. The insets show more details of the electromagnetic field distribution around the apex regions of the nanopyramids. It can be seen from the insets that the hot spots of the nanopyramids range from a few nanometers to a dozen nanometers, and their values decay sharply away from the apex. The intensity of the hot spot is positively correlated with the theoretical EF. The electromagnetic field distribution on the x-y section of sample #1 was also investigated, as shown in Fig. S4. In addition to the highest SERS enhancement in the apex region, the edges of the nanopyramids also exhibit a certain degree of SERS enhancement.

3.2. Analytical EF study of AuNPs substrates with different sizes.

To verify the effect of the nanopyramid size and gap distance on the SERS EF, we fabricated nanopyramidal substrates with sizes of #1 ~ #4 in Fig. 1b by colloidal lithography and a series of micro-nano processes. The tomography of prepared substrates was shown in SEM Figs. 2a ~ 2d, respectively.[34] Nanopyramids showed extremely smooth surfaces.[35] Figs. 2e ~ 2h were the corresponding surface morphology of substrates covered by graphene monolayers (verified in Fig. S3). The colloidal lithography was based on the monolayer of PS microspheres, the diameters of which used for #1 ~ #4 samples were 500 nm, 350 nm, 500 nm and 200 nm, respectively. Benefiting from the careful and precise control, the sizes of the prepared nanopyramids and gap

distances (extracted from the SEM images) were well consistent with the designed ones, as shown in Fig. 2i.

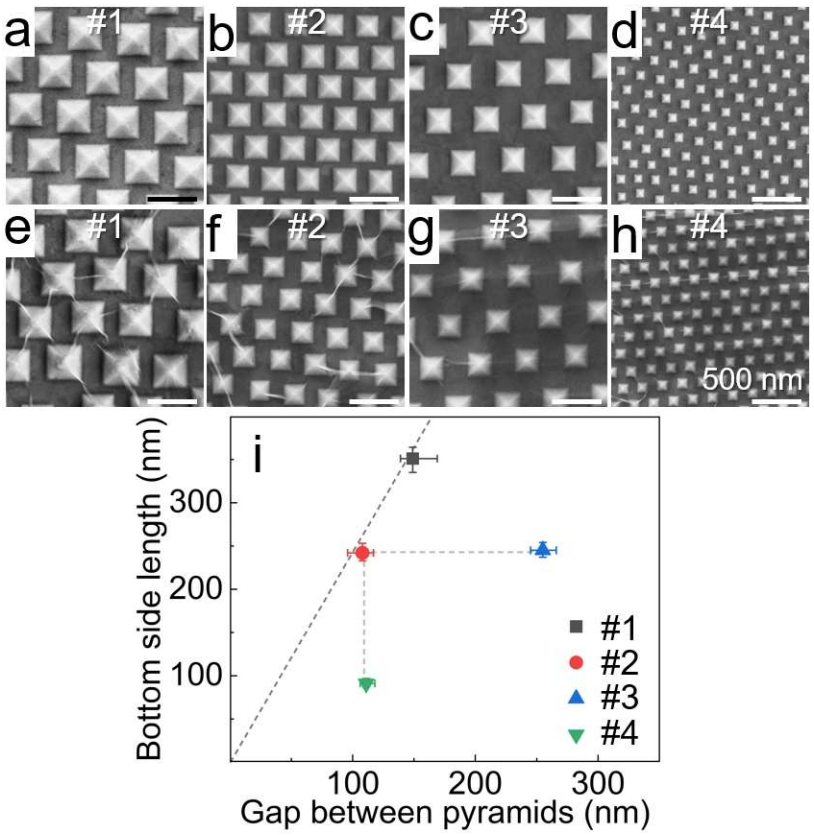

Figure 2. SEM characterization of the prepared substrates. a) ~ d) SEM figures of AuNP substrates with #1 ~ #4 sizes fabricated in this study, respectively. e) ~ f) SEM figures of GAuNP substrates with #1 ~ #4 sizes, respectively. i) Pyramid size characterization of the 4 substrates.

Fig. 3a shows the illustration of protein detection on the graphene-Au nanopyramid hybrid SERS system. The analytical EFs of different substrates were explored by examining R6G as a probe molecule (Fig. S5 ~ S6), and the results were shown in Fig. 3b. The analytical EFs of the AuNPs substrates well agree with the theoretical predictions. The analytical EFs of the GAuNP

substrates are approximately an order of magnitude higher than the AuNP substrates. GAuNP substrate with #1 size shows the highest analytical EF of 1.1×10^{10}, followed by the EFs of substrates with #2, #3 and #4 sizes. The variation trends of the analytical EF of the AuNP and GAuNP substrates with different sizes both agree with that of the theoretical EF (red balls). The detection of protein or polypeptide also supports this observation. Fig. 3c and Fig. 3d reveal SERS spectra of Tau protein and Aβ42 peptide at 10^{-11} M obtained using different GAuNP substrates, respectively. The Raman intensity variations of the protein and peptide are consistent with the EF relationships of the SERS substrates. This demonstrates that the SERS substrates are suitable for protein detection. The #1 size GAuNP hybrid substrate turned out to be the optimal substrate with the strongest EF and thus was used for the subsequent research. Compared with other types of solid substrates, the #1 system also shows superior SERS EFs, as Fig. S8 and Table S4 show.

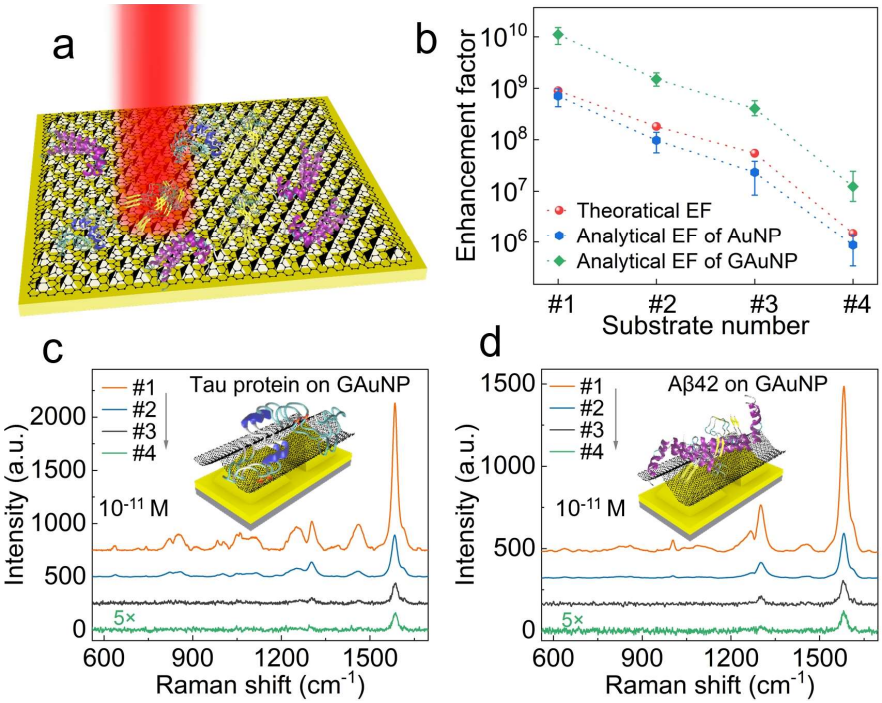

Figure 3. SERS detection using the GAuNPs substrate. a) The schematic diagram of the detection principle. b) The analytical SERS EFs of different substrates for the detection of R6G molecules. c) SERS spectra of 10^{-11} M Tau protein obtained using GAuNPs substrates. d) SERS spectra of 10^{-11} M Aβ42 peptides.

3.3. SERS analysis of Tau and P-Tau protein.

To examine the capability of the GAuNP SERS substrate in clarification of different proteins, Tau and P-Tau were analyzed using the #1 GAuNPs substrate. According to a statistical analysis involving over 2000 individuals, the median concentrations of total Tau protein and P-Tau in the CSF of normal individuals are approximately 3.5×10^{-12} M (230 ng/L) and 5.8×10^{-13} M (38 ng/L), respectively; while these concentrations increase to approximately 9.8×10^{-12} M and 1.3×10^{-12} M in CSF of AD patients, respectively.[36] The Tau and P-Tau protein used in this study are full-length, containing 441 amino acids. This is quite similar to the real situation in CSF of AD patients.[37] Firstly, the detection sensitivity of Tau and P-Tau protein was studied, and the results were shown in Fig. 4a and 4b. The LODs of both Tau and P-Tau proteins reached the lowest concentration of 10^{-15} M, which was more sensitive than LODs of other SERS methods[8, 15] and proceeds the requirement of AD patients' CSF detection. The spectrum of Tau protein is quite similar to that of P-Tau, because the amino acid number and structure of both proteins are almost the same. Tau protein has been considered an intrinsically disordered protein (IDP) with a lack of well-defined secondary structures.[38] To simulate the real situation in the CSF of AD patients as much as possible, Tau and P-Tau with 441 amino acid residues were selected, which were more similar than proteins used in other literature.[14] The 441-residue Tau protein selected in this study has 79 phosphorylation sites, ~8-10 of which are generally phosphorylated in healthy individuals.[8] In the brains of AD patients, Tau protein is phosphorylated at more than 20 sites.[8] In this study, P-Tau protein was

obtained by phosphorylating Tau protein through GSK-3β treatment, which could phosphorylate Tau on Ser199, Thr231, Ser396, Ser400, Ser404, and Ser413.[39] It is noted here that aberrant phosphorylation is a key event triggering the pathological aggregation in AD, because it leads to misfolding and conformational changes of Tau proteins.[39]

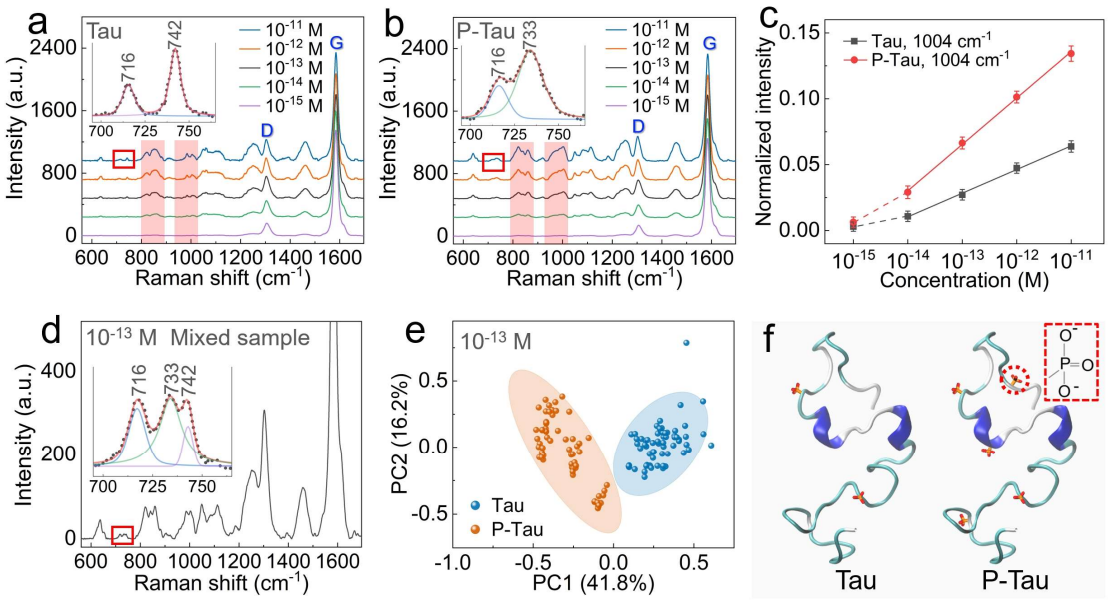

Figure 4. SERS analysis of Tau and P-Tau proteins. a) SERS spectra of Tau protein at different concentrations. b) SERS spectra of P-Tau protein at different concentrations. c) Liner fit (solid line from 10^{-11} M to 10^{-14} M) of the relationship between normalized intensity of the proteins and logarithmic-scale concentrations. The correlation coefficient R^2 is above 0.99. d) SERS spectra of the mixed sample of Tau and P-Tau proteins at 10^{-13} M. e) PCA analysis of Tau and P-Tau proteins at 10^{-13} M. f) Schematic diagram of the structures of Tau and P-Tau proteins. Insets are enlarged views of selected regions in the corresponding figures.

Table 1. Assignment of the Raman peaks of Tau and P-Tau proteins.[40-41]

Raman shift (cm^{-1})	Peak assignment
638	Protein tyrosine (C-C twisting)

716	C-N
733	Phosphate group
742	Tryptophan
822	Tyrosine (Phosphate group)
853	Tyrosine (Ring breathing mode) & Proline (C-C stretch)
860	Tyrosine (Phosphate group)
910	Serine
920	Proline (C-C stretch)
983	Tyrosine
1004	Phenylalanine
1050	Proteins (C-O stretching, C-N stretching)
1061	C-C in-plane bending
1083	Phosphate vibrations
1104	Phenylalanine
1223	Proteins
1237	Amide III & Glycine & Proline
1252	$C\text{-}O_4$ aromatic stretch
1460	Lipids (CH_2/CH_3 deformation)

The obvious differences between the two spectra mainly include changes in some peak shapes and relative intensities, mainly at around 800 cm^{-1} ~ 900 cm^{-1} and 1000 cm^{-1}. Table 1 shows the peak assignment of Tau and P-Tau proteins. Each protein exhibits a characteristic peak, for instance, 742 cm^{-1} (Tryptophan) for Tau protein and 733 cm^{-1} (Phosphate group) for P-Tau protein.[40-41] The above differences may be caused by the slight change in the structure of the P-Tau protein after phosphorylation, which further results in changes in the contacts of certain groups with SERS hotspots. The amide III band mainly reflects N-H in-plane bending and C-N stretching, as well as C_α-C stretching and C=O in-plane bending, and further reflects the conformational changes of proteins.[42] Here the amide III band near 1237 cm^{-1} has been attributed to the residual α-helix structure in the full-length peptide chain.[43]

Graphene is a chemically stable material, and when combined with AuNPs substrates, it enhances biocompatibility. The Raman peak of graphene was therefore used to normalize the

whole spectra, which effectively avoided the Raman intensity fluctuation caused by the heterogeneity of the hot spots, leading to a great enhancement of the quantitative analysis capability of the substrate. Tyrosine, phenylalanine, amide III bands, and C-H, C-N vibrations in organic structures are all strongly expressed. Among them, the peak of phenylalanine at 1004 cm^{-1} remained stable with the conformational changes and was therefore chosen to calibrate the protein concentration. The normalized intensities of the two spectra of proteins were linearly related to the concentration on a logarithmic scale from 10^{-11} M to 10^{-14} M, with a correlation coefficient R^2 above 0.99, as shown in Fig. 4c. This proves the quantitative analysis ability of the hybrid platform. The normalized intensities at 10^{-15} M both deviate upward from the linear relationship because not all hot spots will have adsorbed protein molecules at this ultra-low concentration.[16] In addition, Fig. 4d shows the spectrum of the mixed sample of Tau and P-Tau proteins at 10^{-13} M. The characteristic peaks of both molecules appear in the spectrum, which further suggests the high sensitivity of the GAuNP substrate.

To identify normal Tau protein and P-Tau protein based on SERS spectra, PCA analysis was performed. Fig. 4e shows the classification results based on the full spectrum, and the spectra of the two proteins were divided into two distinct classes (blue and orange ovals) after dimensionality reduction to 2D. All spectra were normalized using the G peak of graphene. In addition, 18 peaks with the greatest difference were also selected from the difference spectrum (Fig. S9) as the input principal components. The PCA results are shown in Fig. S10, where the spectra of Tau and P-Tau proteins were successfully divided into two sets. These results demonstrate the excellent reliability and efficiency of the #1 hybrid SERS substrate in distinguishing proteins with tiny differences at ultra-low concentrations. PCA analysis was also performed on the SERS spectra of the Tau and P-Tau proteins prepared on the #2 hybrid SERS substrate, as shown in Fig. S11. The

results showed that the spectra of Tau and P-Tau protein could not be distinguished by PCA using either the full-spectrum or 18-peaks as inputs. This indicates that the size and structure of the substrate strongly impact the detection results of proteins. Fig. 4f shows a schematic diagram of the intrinsically disordered structures of Tau and P-Tau proteins. P-Tau protein reduces the affinity of protein to microtubules while increasing the aggregation and fibrosis. P-Tau is the main component of AD neurofibrillary tangles.[44]

3.4. SERS analysis of Aβ42 polypeptide.

Both Aβ42 and Aβ40 polypeptides have recently been extensively studied as AD biomarkers, however, Aβ42 has been found a major component of amyloid plaques in AD patients' CSF.[45] Accurate detection of Aβ42 is more meaningful for the diagnosis of AD. The median concentration of Aβ42 in the CSF of normal individuals is 1.8×10^{-10} M (807 ng/L), while for AD patients, the concentration decreases to 1.2×10^{-10} M.[36] Here we used the #1 GAuNP substrate to investigate the Aβ42 polypeptides. As shown in Fig. 5a, the LOD of Aβ42 polypeptide reached 10^{-14} M with an analytical EF of about 2×10^{8} (Fig. S7), which reveals a higher sensitivity than SERS methods reported in literatures[15, 46] and conventional protein detection method ELISA, with a LOD of picograms per milliliter.[47-48] Table 2 shows the peak assignment of Aβ42 peptides. The relationship between the normalized spectral intensity of Aβ42 polypeptide and the concentration was studied. The peak at 1004 cm^{-1} can be assigned to phenylalanine and its normalized intensity is irrelevant to the secondary structure of Aβ42. The normalized intensity of Aβ42 was linearly increased with the concentration in the logarithmic scale, as shown in Fig. 5b.

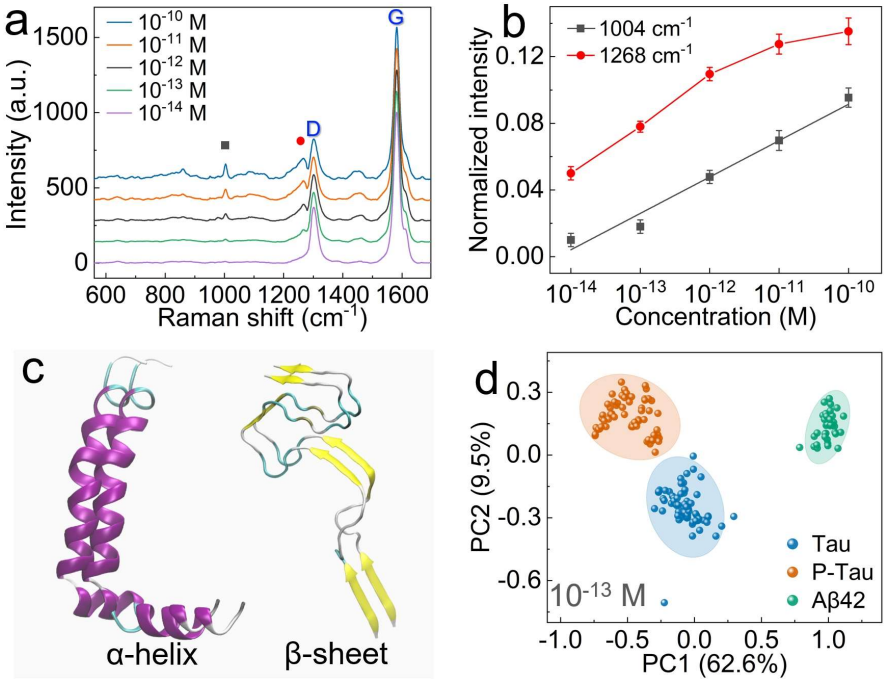

Figure 5. SERS analysis of Aβ42 polypeptide. a) SERS spectra of Aβ42 peptides at different concentrations. b) The relationship between the normalized intensity and concentration in the logarithmic scale of different peaks of Aβ42 peptide. c) Schematic diagram of the α-helix and β-sheet structure of Aβ42 polypeptide. d) PCA analysis of the three biomarkers at 10^{-13} M.

Table 2. Assignment of the Raman peaks of Aβ42 peptides.[41, 49]

Raman shift (cm^{-1})	Peak assignment
683	Tryptophan
831	Tyrosine
859	Tyrosine
950	Valine
980	C-C stretching
1004	Phenylalanine
1090	C-C stretch
1268	Amide III
1455	CH_2 deformation

The broadband near 1268 cm^{-1} can be assigned to the amide III band, which is associated with the conformational change of Aβ polypeptides. At lower concentrations ($<10^{-12}$ M), the normalized intensity of the amide III band linearly increased with the concentration in the logarithmic scale, which is mainly due to the α-helical structure of the Aβ protein.[42] The α-helix is the right-handed helical conformation of the protein (as shown in Fig. 5c) formed by hydrogen bonds between the backbone N-H and C=O groups.[50] The normalized intensity of the amide III band deviates downward from the linear direction with increasing Aβ protein concentration. This is mainly due to the secondary structure transition from α-helix to β-sheet in some Aβ42 polypeptides. The original α-helical structure of Aβ42 is susceptible to misfolding, and this misfolding is considered to be the first step in the process of Aβ oligomerization, polymerization, and fibrillation.[51] Misfolded proteins often interact with other normal proteins and further cause them to transit into a neurotoxic misfolded state, and this is the reason why they are often referred to as infectious conformations.[52] In this study, when the concentration of Aβ polypeptides was low, almost all the peptides were in the α-helical structure, and the normalized intensity of 1268 cm^{-1} linearly increased with the concentration in the logarithmic scale. However, as the peptide concentration increased, the amount of misfolded Aβ (β-sheet secondary structure) increased, and thus the misfolded protein infected other normal proteins. The β-sheet structure peptide contributes less to the intensity of the amide III band, resulting in a downward deviation of the normalized peak intensity at 1268 cm^{-1} from the linear increasing relationship.[15] Fig. S13 shows the Raman spectrum change of Aβ42 with time.

Fig. 5c illustrates a schematic diagram of the secondary structure of Aβ42 polypeptides. Different from the α-helix structure with the right-handed helical feature, the β-sheet conformation is formed by the lateral aggregation of two or more nearly fully extended peptide chains, with the

formation of regular hydrogen bonds between N-H and C=O groups on the adjacent backbones.[53] Further mixed solution testing was conducted using Aβ42 peptide and Tau protein mixtures at 10^{-13} M, and the results are shown in Fig. S14. The spectra of mixed samples involve peaks unique to Tau protein, Aβ42 peptide, as well as those shared by both. PCA analysis was then performed on spectra of the three biomarkers, and the results were shown in Fig. 5d, where the biomarkers were correctly and clearly classified into three sets. The principal components are the linear combinations of the original input variables and maximize the preservation of the original dataset information. The smaller projection lengths of the Aβ42 peptide in the PC1 and PC2 axis correspond to the more monotonic SERS spectra, which are determined by fewer amino acids of the peptide. In addition, Aβ polypeptides at different concentrations were also analyzed by PCA method to reveal the structural changes of Aβ42 peptide. Table 3 shows the sensitivity and accuracy values of different biomarkers. Sensitivity is defined as the true positive rate or number of correctly identified analytes, and specificity is defined as the true negative rate. The high sensitivity and specificity demonstrate the effectiveness of the strategy in distinguishing the AD biomarkers. As shown in Fig. S12, spectra at different concentrations have been correctly classified by the PCA analysis of both the full spectrum and the 18 peaks spectrum. The dimensionality-reduced point set also reveals the original structure information of Aβ42 at different concentrations. Fig. S12 shows that when the concentration reaches 10^{-11} M and 10^{-10} M, the dispersion of the 2D point set significantly increases. This is related to the fact that at this concentration, Aβ42 peptides have a mixture of α-helix and β-sheet structures. The quantitatively high-sensitive quantitative detection, conformational analysis and protein species identification of three proteins (or polypeptides) pave the way to the practical application of SERS for the detection

of protein biomarkers for early diagnosis of AD. In addition, this SERS platform can be further extended to other peptide and protein biomarkers detection for a range of disease diagnostics.

Table 3. Sensitivity and accuracy of different biomarkers.

Analyte	Sensitivity (%)	Accuracy (%)
Tau protein	100	97.0
P-Tau protein	100	100
Aβ42 peptide	100	99.2

4. Conclusion

In conclusion, we reported the label-free detection with high sensitivity and specification of three AD biomarkers, i.e. Tau, P-Tau and Aβ42 peptides using the graphene-Au pyramids hybrid SERS platform. The impact of nanopyramid size and gap distance on the SERS EF was studied by FDTD simulations and experimental validations. The SERS EF was found to be facilitated by larger pyramid size and smaller gap distance. The optimized #1 GAuNP substrate shows a high analytical EF of 1.1×10^{10}. Such hybrid SERS substrates exhibit ultra-sensitivity, with LOD of 10^{-15} M for Tau (P-Tau) proteins and 10^{-14} M for Aβ42 peptide, respectively. PCA analysis correctly categorized the SERS spectra of normal and phospho-Tau proteins as well as the Aβ peptide using the pattern-optimized substrate. Amide III bands located at different Raman shifts indicate different structural conformations of the detected proteins or polypeptides. For Aβ42, the normalized intensity of the amide III band at 1268 cm^{-1} deviated downward from the linear increasing relationship, which was attributed to the secondary structure transition of some Aβ polypeptides from α-helix to β-sheet when the concentration increased. These results demonstrate that the GAuNP hybrid SERS platform can potentially serve as an addition or alternative to traditional analytical methods for the assistance of early diagnosis of AD.

ASSOCIATED CONTENT

Supporting Information.

The following files are available free of charge.

Schematic illustration of the AuNPs substrate fabrication process; Critical nanopyramid dimensions corresponding to two types of different pyramid alignments; Characterization of graphene monolayer properties; The electromagnetic field distributions on the x-y cross-sections of the nanopyramidal substrate #1 at different height horizontal planes; SERS spectra of R6G; Raman spectrum of R6G on flat Au film; SERS (10^{-15} M) and Raman (10^{-6} M) spectra of Tau protein and Aβ42 peptide; SERS EF comparison of solid substrates; The difference spectrum; PCA results of Tau and P-Tau proteins using 18 peaks as inputs; PCA results of spectra of Tau and P-Tau proteins obtained from #2 graphene-Au nanopyramid substrate; PCA results of Aβ42 polypeptides at different concentrations; Change of Aβ42 Raman spectrum with time; SERS spectra of the mixed sample of Tau protein and Aβ42 peptide at 10^{-13} M. (PDF)

AUTHOR INFORMATION

Corresponding Author

*Zhen Xie - The college of Life Sciences and Medicine, Northwest University, No. 229 Taibai North Road, Xi'an, Shaanxi, 710069, P.R. China; E-mail: xiezhenhh@163.com.

*Libo Zhao - School of Instrument Science and Technology, State Key Laboratory for Manufacturing Systems Engineering & The International Joint Laboratory for Micro/Nano Manufacturing and Measurement Technology, Xi'an Jiaotong University,Xi'an, 710049, China; E-mail: libozhao@mail.xjtu.edu.cn

*Gang Zhao - The college of Life Sciences and Medicine, Northwest University, No. 229 Taibai North Road, Xi'an, Shaanxi, 710069, P.R. China; E-mail: zhaogang@nwu.edu.cn.

*Wei Ren - State Key Laboratory for Manufacturing Systems Engineering; Electronic Materials Research Laboratory, Key Laboratory of the Ministry of Education, School of Electronic Science and Engineering, Xi'an Jiaotong University, 710049 Xi'an, China; Email: wren@mail.xjtu.edu.cn.

*Gang Niu - State Key Laboratory for Manufacturing Systems Engineering; Electronic Materials Research Laboratory, Key Laboratory of the Ministry of Education, School of Electronic Science and Engineering, Xi'an Jiaotong University, 710049 Xi'an, China; Email: gangniu@xjtu.edu.cn.

Author

Heping Wu – State Key Laboratory for Manufacturing Systems Engineering; Electronic Materials Research Laboratory, Key Laboratory of the Ministry of Education, School of Electronic Science and Engineering, Xi'an Jiaotong University, 710049 Xi'an, China

Yan Duan - The college of Life Sciences and Medicine, Northwest University, No. 229 Taibai North Road, Xi'an, Shaanxi, 710069, P.R. China

Luyue Jiang – State Key Laboratory for Manufacturing Systems Engineering; Electronic Materials Research Laboratory, Key Laboratory of the Ministry of Education, School of Electronic Science and Engineering, Xi'an Jiaotong University, 710049 Xi'an, China

Xinhao Cao - State Key Laboratory for Manufacturing Systems Engineering; Electronic Materials Research Laboratory, Key Laboratory of the Ministry of Education, School of Electronic Science and Engineering, Xi'an Jiaotong University, 710049 Xi'an, China

Yi Quan - School of Microelectronics, Xidian University, Xi'An, 710071, China

Matthew Xinhu Ren - Biology Program, Faculty of Science, The University of British Columbia, Vancouver, BC V6T 1Z4, Canada

Shengli Wu - Key Laboratory of Physical Electronics and Devices, Ministry of Education, School of Electronic Science and Engineering, Xi'an Jiaotong University, Xi'an, 710049, China

Nan Zhang – State Key Laboratory for Manufacturing Systems Engineering; Electronic Materials Research Laboratory, Key Laboratory of the Ministry of Education, School of Electronic Science and Engineering, Xi'an Jiaotong University, 710049 Xi'an, China

Zhugen Yang - School of Water, Energy and Environment, Cranfield University, Cranfield, MK43 0AL, UK

Zhuangde Jiang - The State Key Laboratory for Manufacturing Systems Engineering & The International Joint Laboratory for Micro/Nano Manufacturing and Measurement Technology, Xi'an Jiaotong University, Xi'an 710049, China

Author Contributions

G.Z., W.R., L.Z, Z.X. and G.N. designed the work. H. W. performed the FDTD simulation and the experiments including the fabrication of different substrates and Raman detection. Y.Q. and Z.J. helped the design and fabrication of the hybrid SERS substrates. Y. D. and L. J. performed part of the Raman test. C. H., M.X.R, S.W. and N.Z. performed part of the PCA analysis. Z.X., Z.Y. and Y.D. carried out partly the protein analysis and structure study. All the co-authors discussed the results and revised the manuscript.

Funding Sources

The authors thank Postdoctoral Fellowship Program of CPSF (GZC20232096), Postdoctoral Research Project of Shaanxi Province (2023BSHEDZZ59), Key R&D Program of Shaanxi Province of China (2020GY-271), The Fundamental Research Funds for the Central Universities (xzd012020059), The “111 Project” of China (B14040).

Notes

The authors declare no competing interest.

ACKNOWLEDGMENT

We acknowledge Mrs. Dan He at the Instrument Analysis Center of Xi’an Jiaotong University for the assistance with Raman analysis.

REFERENCES

(1) Wisniewski, T.;Goni, F. Immunotherapeutic approaches for Alzheimer's disease. *Neuron* **2015,** *85* (6), 1162-76.
(2) Breijyeh, Z.;Karaman, R. Comprehensive Review on Alzheimer's Disease: Causes and Treatment. *Molecules* **2020,** *25* (24), 5789-5816.
(3) Vina, J.;Sanz-Ros, J. Alzheimer's disease: Only prevention makes sense. *Eur. J. Clin. Invest.* **2018,** *48* (10), e13005.
(4) Johnson, K. A.; Fox, N. C.; Sperling, R. A.;Klunk, W. E. Brain Imaging in Alzheimer Disease. *Cold Spring Harb. Perspect. Med.* **2012,** *2* (4), a006213-a006213.
(5) Chapman, R. M.; Mapstone, M.; Porsteinsson, A. P.; Gardner, M. N.; McCrary, J. W.; DeGrush, E.; Reilly, L. A.; Sandoval, T. C.;Guillily, M. D. Diagnosis of Alzheimer's disease using neuropsychological testing improved by multivariate analyses. *J. Clin. Exp. Neuropsychol.* **2010,** *32* (8), 793-808.
(6) Jack, C. R., Jr.;Holtzman, D. M. Biomarker modeling of Alzheimer's disease. *Neuron* **2013,** *80* (6), 1347-58.
(7) Scheltens, P.; Blennow, K.; Breteler, M. M. B.; de Strooper, B.; Frisoni, G. B.; Salloway, S.;Van der Flier, W. M. Alzheimer's disease. *Lancet* **2016,** *388* (10043), 505-517.
(8) Zengin, A.; Tamer, U.;Caykara, T. A SERS-based sandwich assay for ultrasensitive and selective detection of Alzheimer's tau protein. *Biomacromolecules* **2013,** *14* (9), 3001-9.
(9) Cohen, L.;Walt, D. R. Highly Sensitive and Multiplexed Protein Measurements. *Chem. Rev.* **2018,** *119* (1), 293-321.
(10) Bai, S.; Ren, X.; Obata, K.; Ito, Y.;Sugioka, K. Label-free trace detection of bio-molecules by liquid-interface assisted surface-enhanced Raman scattering using a microfluidic chip. *Opto-electron. adv.* **2022,** *5* (10), 210121-210121.

(11) Shao, M.; Ji, C.; Tan, J.; Du, B.; Zhao, X.; Yu, J.; Man, B.; Xu, K.; Zhang, C.;Li, Z. Ferroelectrically modulate the Fermi level of graphene oxide to enhance SERS response. *Opto-electron. adv.* **2023,** *6* (11), 230094-230094.
(12) Zong, C.; Xu, M.; Xu, L.-J.; Wei, T.; Ma, X.; Zheng, X.-S.; Hu, R.;Ren, B. Surface-Enhanced Raman Spectroscopy for Bioanalysis: Reliability and Challenges. *Chem. Rev.* **2018,** *118* (10), 4946-4980.
(13) Zhu, K.; Wang, Z.; Zong, S.; Liu, Y.; Yang, K.; Li, N.; Wang, Z.; Li, L.; Tang, H.;Cui, Y. Hydrophobic Plasmonic Nanoacorn Array for a Label-Free and Uniform SERS-Based Biomolecular Assay. *ACS Appl. Mater. Interfaces* **2020,** *12* (26), 29917-29927.
(14) Ma, H.; Liu, S.; Liu, Y.; Zhu, J.; Han, X. X.; Ozaki, Y.;Zhao, B. In-situ fingerprinting phosphorylated proteins via surface-enhanced Raman spectroscopy: Single-site discrimination of Tau biomarkers in Alzheimer's disease. *Biosens. Bioelectron.* **2021,** *171*, 112748.
(15) Park, H. J.; Cho, S.; Kim, M.;Jung, Y. S. Carboxylic Acid-Functionalized, Graphitic Layer-Coated Three-Dimensional SERS Substrate for Label-Free Analysis of Alzheimer's Disease Biomarkers. *Nano Lett.* **2020,** *20* (4), 2576-2584.
(16) Yu, X.; Hayden, E. Y.; Wang, P.; Xia, M.; Liang, O.; Bai, Y.; Teplow, D. B.;Xie, Y. H. Ultrasensitive amyloid β‐protein quantification with high dynamic range using a hybrid graphene–gold surface‐enhanced Raman spectroscopy platform. *J. Raman Spectrosc.* **2019,** *51* (3), 432-441.
(17) Yu, X.; Hayden, E. Y.; Xia, M.; Liang, O.; Cheah, L.; Teplow, D. B.;Xie, Y. H. Surface enhanced Raman spectroscopy distinguishes amyloid Β‐protein isoforms and conformational states. *Protein Sci.* **2018,** *27* (8), 1427-1438.
(18) Yu, X.; Srivastava, S.; Huang, S.; Hayden, E.; Teplow, D.;Xie, Y.-H. The Feasibility of Early Alzheimer's Disease Diagnosis Using a Neural Network Hybrid Platform. *Biosensors* **2022,** *12* (9), 753-762.
(19) Pei, Z.; Li, J.; Ji, C.; Tan, J.; Shao, Z.; Zhao, X.; Li, Z.; Man, B.; Yu, J.;Zhang, C. Flexible Cascaded Wire-in-Cavity-in-Bowl Structure for High-Performance and Polydirectional Sensing of Contaminants in Microdroplets. *J. Phys. Chem. Lett.* **2023,** *14* (25), 5932-5939.
(20) Lin, T.-H.; Linn, N. C.; Tarajano, L.; Jiang, B.;Jiang, P. Electrochemical SERS at periodic metallic nanopyramid arrays. *J. Phys. Chem. C* **2009,** *113* (4), 1367-1372.
(21) Sun, C.-H.; Linn, N. C.;Jiang, P. Templated Fabrication of Periodic Metallic Nanopyramid Arrays. *Chem. Mater.* **2007,** *19* (18), 4551-4556.
(22) Wu, H.; Niu, G.; Ren, W.; Jiang, L.; Liang, O.; Zhao, J.; Liu, Y.;Xie, Y. H. Crucial impact of hydrophilicity on the self-assemble 2D colloidal crystals using Langmuir-Blodgett method. *Langmuir* **2020,** *36* (34), 10061-10068.
(23) Wang, P.; Xia, M.; Liang, O.; Sun, K.; Cipriano, A. F.; Schroeder, T.; Liu, H.;Xie, Y.-H. Label-free SERS selective detection of dopamine and serotonin using graphene-Au nanopyramid heterostructure. *Anal. Chem.* **2015,** *87* (20), 10255-10261.
(24) Wu, H.; Niu, G.; Ren, W.; Jiang, L.; Zhao, J.; Quan, Y.; Ren, M. X.; Yu, W.; Zhang, Y.; Cao, X.; Liu, Y.; An, R.; Dai, L.; Wang, Z.; Zhao, L.; Xie, Z.;Zhao, G. Highly sensitive label-free detection of analytes at different scales using uniform graphene-nanopyramids hybrid SERS system. *Sens. Actuators, B* **2022,** *354*, 131205-131214.
(25) Wu, H.; Niu, G.; Ren, W.; Yang, Z.; Xu, Q.; Dai, L.; Jiang, L.; Zhai, S.; Zhao, J.; Zhang, N.; Zhao, L.; Jiang, Z.;Zhao, G. Large-Area and Clean Graphene Transfer on Gold-Nanopyramid-Structured Substrates: Implications for Surface-Enhanced Raman Scattering Detection. *ACS Appl. Nano Mater.* **2022,** *5* (6), 3878-3888.

(26) Fang, P.-P.; Li, J.-F.; Yang, Z.-L.; Li, L.-M.; Ren, B.;Tian, Z.-Q. Optimization of SERS activities of gold nanoparticles and gold-core-palladium-shell nanoparticles by controlling size and shell thickness. *J. Raman Spectrosc.* **2008,** *39* (11), 1679-1687.
(27) Falkovsky, L. A. Optical properties of graphene. *J. Phys.: Conf. Ser.* **2008,** *129*, 012004.
(28) Barchiesi, D.;Grosges, T. Fitting the optical constants of gold, silver, chromium, titanium, and aluminum in the visible bandwidth. *J. Nanophotonics* **2014,** *8* (1), 083097-083112.
(29) Luo, S. C.; Sivashanmugan, K.; Liao, J. D.; Yao, C. K.;Peng, H. C. Nanofabricated SERS-active substrates for single-molecule to virus detection in vitro: a review. *Biosens. Bioelectron.* **2014,** *61*, 232-40.
(30) Zeng, Z.; Liu, Y.;Wei, J. Recent advances in surface-enhanced raman spectroscopy (SERS): Finite-difference time-domain (FDTD) method for SERS and sensing applications. *TrAC Trend. Anal. Chem.* **2016,** *75*, 162-173.
(31) Yang, Z.; Li, Q.; Ruan, F.; Li, Z.; Ren, B.; Xu, H.;Tian, Z. FDTD for plasmonics: Applications in enhanced Raman spectroscopy. *Chin. Sci. Bull.* **2010,** *55* (24), 2635-2642.
(32) Le Ru, E. C.; Grand, J.; Félidj, N.; Aubard, J.; Lévi, G.; Hohenau, A.; Krenn, J. R.; Blackie, E.;Etchegoin, P. G. Experimental Verification of the SERS Electromagnetic Model beyond the |E|4 Approximation: Polarization Effects. *J. Phys. Chem. C* **2008,** *112* (22), 8117-8121.
(33) Meng, X.; Wang, H.; Chen, N.; Ding, P.; Shi, H.; Zhai, X.; Su, Y.;He, Y. A Graphene–Silver Nanoparticle–Silicon Sandwich SERS Chip for Quantitative Detection of Molecules and Capture, Discrimination, and Inactivation of Bacteria. *Anal. Chem.* **2018,** *90* (9), 5646-5653.
(34) Luo, S.; Guo, H.; Zhang, S.; Wang, Z.; Li, X.; Peng, W.; Wang, J.;Yan, G. Efficient production of metal manganese achieved by cylindrical and rotary electrode. *J. Clean. Prod.* **2021,** *326*, 129266-129274.
(35) Wang, Y.; Xue, Y.;Zhang, C. Electrochemical product engineering towards sustainable recovery and manufacturing of critical metals. *Green Chem.* **2021,** *23* (17), 6301-6321.
(36) Dorey, A.; Perret-Liaudet, A.; Tholance, Y.; Fourier, A.;Quadrio, I. Cerebrospinal Fluid Aβ40 Improves the Interpretation of Aβ42 Concentration for Diagnosing Alzheimer's Disease. *Front. Neurol.* **2015,** *6*.
(37) Beurel, E.; Grieco, S. F.;Jope, R. S. Glycogen synthase kinase-3 (GSK3): regulation, actions, and diseases. *Pharmacol. Ther.* **2015,** *148*, 114-31.
(38) Ambadipudi, S.; Biernat, J.; Riedel, D.; Mandelkow, E.;Zweckstetter, M. Liquid–liquid phase separation of the microtubule-binding repeats of the Alzheimer-related protein Tau. *Nat. Commun.* **2017,** *8* (1), 275.
(39) Kolarova, M.; Garcia-Sierra, F.; Bartos, A.; Ricny, J.;Ripova, D. Structure and pathology of tau protein in Alzheimer disease. *Int. J. Alzheimers Dis.* **2012,** *2012*, 731526.
(40) Fujihara, J.; Fujita, Y.; Yamamoto, T.; Nishimoto, N.; Kimura-Kataoka, K.; Kurata, S.; Takinami, Y.; Yasuda, T.;Takeshita, H. Blood identification and discrimination between human and nonhuman blood using portable Raman spectroscopy. *Int. J. Legal Med.* **2016,** *131* (2), 319-322.
(41) Movasaghi, Z.; Rehman, S.;Rehman, I. U. Raman Spectroscopy of Biological Tissues. *Appl. Spectrosc. Rev.* **2007,** *42* (5), 493-541.
(42) Herrero, A. M. Raman Spectroscopy for Monitoring Protein Structure in Muscle Food Systems. *Crit. Rev. Food Sci. Nutr.* **2008,** *48* (6), 512-523.
(43) Kunjithapatham, R.; Oliva, F. Y.; Doshi, U.; Perez, M.; Avila, J.;Munoz, V. Role for the alpha-helix in aberrant protein aggregation. *Biochemistry* **2005,** *44* (1), 149-56.

(44) Alonso, A. C.; Grundke-Iqbal, I.;Iqbal, K. Alzheimer's disease hyperphosphorylated tau sequesters normal tau into tangles of filaments and disassembles microtubules. *Nat. Med.* **1996,** *2* (7), 783-7.
(45) Gu, L.;Guo, Z. Alzheimer's Aβ42 and Aβ40 peptides form interlaced amyloid fibrils. *J. Neurochem.* **2013,** *126* (3), 305-311.
(46) Xia, Y.; Padmanabhan, P.; Sarangapani, S.; Gulyás, B.;Vadakke Matham, M. Bifunctional Fluorescent/Raman Nanoprobe for the Early Detection of Amyloid. *Sci. Rep.* **2019,** *9* (1), 8497.
(47) Jensen, M.; Hartmann, T.; Engvall, B.; Wang, R.; Uljon, S. N.; Sennvik, K.; Näslund, J.; Muehlhauser, F.; Nordstedt, C.; Beyreuther, K.;Lannfelt, L. Quantification of Alzheimer Amyloid β Peptides Ending at Residues 40 and 42 by Novel ELISA Systems. *Mol. Med.* **2000,** *6* (4), 291-302.
(48) Perez-Grijalba, V.; Fandos, N.; Canudas, J.; Insua, D.; Casabona, D.; Lacosta, A. M.; Montanes, M.; Pesini, P.;Sarasa, M. Validation of Immunoassay-Based Tools for the Comprehensive Quantification of Abeta40 and Abeta42 Peptides in Plasma. *J. Alzheimers Dis.* **2016,** *54* (2), 751-62.
(49) De Gelder, J.; De Gussem, K.; Vandenabeele, P.;Moens, L. Reference database of Raman spectra of biological molecules. *J. Raman Spectrosc.* **2007,** *38* (9), 1133-1147.
(50) Anand, P.; Nandel, F. S.;Hansmann, U. H. E. The Alzheimer's β amyloid (Aβ1–39) monomer in an implicit solvent. *The Journal of Chemical Physics* **2008,** *128* (16), 165102.
(51) Chong, S.-H.;Ham, S. Distinct Role of Hydration Water in Protein Misfolding and Aggregation Revealed by Fluctuating Thermodynamics Analysis. *Acc. Chem. Res.* **2015,** *48* (4), 956-965.
(52) Chaudhuri, T. K.;Paul, S. Protein‐misfolding diseases and chaperone‐based therapeutic approaches. *The FEBS Journal* **2006,** *273* (7), 1331-1349.
(53) Sato, T.; Kienlen-Campard, P.; Ahmed, M.; Liu, W.; Li, H.; Elliott, J. I.; Aimoto, S.; Constantinescu, S. N.; Octave, J. N.;Smith, S. O. Inhibitors of amyloid toxicity based on beta-sheet packing of Abeta40 and Abeta42. *Biochemistry* **2006,** *45* (17), 5503-16.